

# Floquet-engineering and simulating exceptional rings with a quantum spin system

Peng He<sup>1,\*</sup> and Ze-Hao Huang<sup>1</sup>

<sup>1</sup>*National Laboratory of Solid State Microstructures and School of Physics, Nanjing University, Nanjing 210093, China*  
(Dated: December 22, 2024)

Time-periodic driving in the form of coherent radiation provides powerful tool for the manipulation of topological materials or synthetic quantum matter. In this paper we propose a scheme to realize non-Hermitian semimetals exhibiting exceptional rings in the spectra through Floquet engineering. A transition from a concentric pair of the rings to a dipolar pair is observed. The concentric pair only carries a quantized Berry phase while the dipolar pair possesses opposite Chern numbers in addition, signaling a topological Lifshitz transition of the Fermi surface. The transport properties of the system are addressed, and we find that this transition process is accompanied by the emergency of a nontrivial Hall conductivity. Furthermore, we explore the quantum simulation of non-Hermitian semimetals with a quantum spin system and the characterization of the topology via the long-time dynamics.

*Introduction.*— Exceptional points (EPs) are defective degeneracies in the energy spectra where the eigenstates of the Hamiltonian do not span a complete Hilbert space [1–3]. They are fascinating instances of non-Hermitian (NH) systems emerging as effective description of non-conserved systems such as solids with finite quasi-particle lifetimes [4–7], disordered Dirac fermions [8, 9], and artificial lattice with gain/loss or nonreciprocity [10–15]. Recently, the existence of different exceptional solutions, such as isolated EPs [16], exceptional rings (ERs) [17–19], exceptional links [20–22] and exceptional surfaces [23–25] in NH semimetals and their topological nature have been recognized [26–30]. The intriguing features of the topology include that new symmetries [28] and topology invariants such as energy vorticity [27] and discriminant number [31], anomalous skin effect [32–37], and the breakdown of the usual bulk-boundary correspondence [32, 38–41]. Furthermore, certain discrete symmetries are required to stabilize the 1D line nodes of a 3D Hermitian topological semimetal as a result of Bott periodicity for even-odd dichotomy [42, 43], while the exceptional line in NH semimetal is stable even without the imposition of any protecting symmetry [20, 21].

For conventional topological materials or synthetic quantum matters [44], a change in the structure of Fermi surface may happen when an external field is applied. For instance, the Dirac points in graphene can move under the changes of control parameters [45–48]; periodical drives can give rise to a dimension deformation from nodal line to Weyl points attached with a  $\mathbb{Z}$ -monopole charge [49–52], incorporating the coherent manipulation of topological semimetals into the various contexts of Floquet topological matters [53, 54]. Furthermore, the non-Hermiticity has also been included in the field of Floquet states in topological insulators and superconductors [55–57]. In this paper, we propose the realization of exceptional ring semimetals by generalizing the Floquet-engineering methods developed in Ref. [49–52, 61, 62] to

NH cases. The NH semimetal exhibiting double ERs is driven by a circularly polarized light. And a transition of the ERs from a concentric pair of which each one only carries a nontrivial Berry phase to a dipolar pair with opposite Chern numbers is observed. This signals an exotic topological Lifshitz transition which has no Hermitian counterpart. Furthermore, we find that this transition process is accompanied by the emergency of a nontrivial Hall conductivity, which provides experimentally observable evidence for the change of the Fermi surface.

On the other hand, the experimental demonstration and quantum simulation of the NH quantum mechanics has been attracted considerable interest in recent years. Particularly promising approaches using different platform have been successfully performed. One line of works is engineering the Lindblad master equation using acoustics [63, 64], optical [14, 15, 65, 66] or atomic [11, 44, 67, 68] systems. Other novel protocols adopt alternative methods with no need of controlling an open system [69–71] and recently successfully carried out with a single nitrogen-vacancy (NV) center in diamond [72, 73]. In these protocols the NH Hamiltonians emerge as an effective description of subsystem for a larger dilated Hermitian system. We adopt this dilation formalism to simulate the NH nodal-line semimetal. In principle, the eigen-energies of NH Hamiltonian can be revealed from the dynamical phase, and the topological properties of the exceptional degeneracies can be reconstructed from the time-averaged spin textures.

*Floquet-engineering of exceptional ring.*— We start with considering the model Hamiltonian exhibiting double exceptional rings,

$$\hat{H}_{\mathbf{k}} = \sum_{\mathbf{k}} \hat{\Psi}_{\mathbf{k}}^{\dagger} \mathcal{H}(\mathbf{k}) \hat{\Psi}_{\mathbf{k}} + \sum_{\mathbf{k},\sigma} i \hat{c}_{\mathbf{k},\sigma} \xi^{\dagger} + i \hat{c}_{\mathbf{k},\sigma}^{\dagger} \xi, \quad (1)$$

where  $\hat{\Psi}_{\mathbf{k}} = (\hat{c}_{\mathbf{k},a}, \hat{c}_{\mathbf{k},b})^T$  and  $a, b$  refer to the two orbitals involved;  $\mathcal{H}(\mathbf{k}) = (m - Bk^2)\tau_x + vk_z\tau_z + i\gamma\tau_z$  with  $k^2 = k_x^2 + k_y^2 + k_z^2$  and  $\tau_{x,y,z}$  are Pauli matrices;  $\xi$  and  $\xi^{\dagger}$  are the Langevin noise operators, and they satisfy  $\langle \xi_j(t) \xi_l^{\dagger}(t') \rangle_{\text{noise}} = 2\gamma \delta_{jl} \delta(t-t')$ ,  $\langle \xi_j^{\dagger}(t) \xi_l^{\dagger}(t') \rangle_{\text{noise}} = 0$  [78, 79].

\*Electronic address: [hep@smail.nju.edu.cn](mailto:hep@smail.nju.edu.cn)

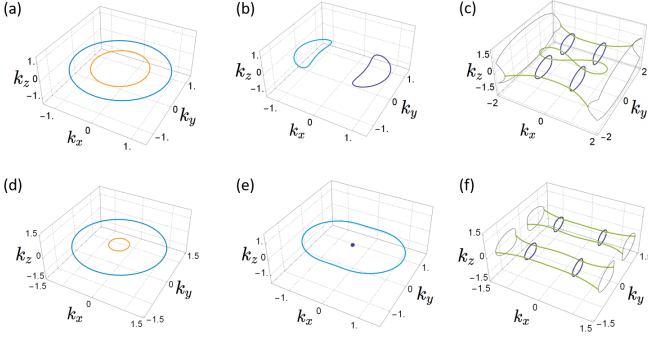


FIG. 1: The band structure as computed from the Hamiltonian in Eq.(6) with  $\tilde{m} = 1$ ,  $B = 1$ ,  $v = 1$ ,  $\phi = 0$ , (a-c)  $\gamma = 0.5$  and (d-f)  $\gamma = 0.9$ ; the frequency of the periodic driving (a,d)  $\omega/A = 10$ , (b,e)  $\omega/A = 3$ , (c,f)  $\omega/A = 1$ . For simplicity we have taken  $B = v = e = 1$ .

We consider periodic drive by application of light beam which generates a vector potential  $\mathbf{A}(t) = A[0, \cos(\omega t), \sin(\omega t)]$ . The time-dependent Hamiltonian under the external field can be obtained by the minimal coupling prescription  $\mathcal{H}(\mathbf{k}) \rightarrow \mathcal{H}(\mathbf{k} + e\mathbf{A})$ . In the high frequency regime, the Floquet Hamiltonian can be computed in a perturbative manner. We follow the standard procedures to expand the prescribed Hamiltonian in orders of  $1/\omega$  as  $\mathcal{H}(t, \mathbf{k}) = \sum_n \mathcal{H}_n e^{in\omega t}$ ,

$$\begin{aligned} \mathcal{H}_0(\mathbf{k}) &= [m - Be^2 A_0^2 - Bk^2] \Psi_{\mathbf{k}}^\dagger \tau_x \Psi_{\mathbf{k}} + (vk_z + i\gamma) \Psi_{\mathbf{k}}^\dagger \tau_z \Psi_{\mathbf{k}}, \\ \mathcal{H}_{\pm 1}(\mathbf{k}) &= -eA_0 [2B(k_y \mp ie^{\pm i\phi} k_z) \Psi_{\mathbf{k}}^\dagger \tau_x \Psi_{\mathbf{k}} \\ &\quad \pm ie^{\pm i\phi} v \Psi_{\mathbf{k}}^\dagger \tau_z \Psi_{\mathbf{k}}] / 2, \\ \mathcal{H}_{\pm 2}(\mathbf{k}) &= -Be^2 A_0^2 (1 - e^{\pm i2\phi}) \Psi_{\mathbf{k}}^\dagger \tau_x \Psi_{\mathbf{k}} / 4, \end{aligned} \quad (2)$$

and  $\mathcal{H}_n = 0$  for  $|n| > 2$ . For the Floquet-engineering of a non-Hermitian system, the effective time-independent Hamiltonian takes a slightly different form [81],

$$\begin{aligned} \mathcal{H}_{\text{eff}}(\mathbf{k}) &= \mathcal{H}_0 + \sum_{n \geq 1} \frac{[\mathcal{H}_{+n}, \mathcal{H}_{-n}]}{n\omega} + \\ &\quad \sum_{n, \sigma} s \frac{2i\gamma}{\omega^2} [\mathcal{H}_n, \hat{c}_{\mathbf{k}, \sigma}]^\dagger [\mathcal{H}_n, \hat{c}_{\mathbf{k}, \sigma}], \end{aligned} \quad (3)$$

where  $s = \tau_z(\hat{c}_{\mathbf{k}, \sigma}|0\rangle) = \pm 1$ , and the last term describes a micromotion. The first two terms lead to

$$\mathcal{H}_P = [\tilde{m} - Bk^2] \tau_x + (vk_z + i\gamma) \tau_z + \lambda k_y \tau_y, \quad (4)$$

where  $\lambda = -2e^2 BvA^2 \cos(\phi)/\omega$  and  $\tilde{m} = m - Be^2 A^2$ , while the micromotion term gives rise to nontrivial second order contributions,

$$\begin{aligned} \sum_{\sigma} [\mathcal{H}_1, \hat{c}_{\mathbf{k}, \sigma}]^\dagger [\mathcal{H}_1, \hat{c}_{\mathbf{k}, \sigma}] &= \sum_{\sigma} [\mathcal{H}_{-1}, \hat{c}_{\mathbf{k}, \sigma}]^\dagger [\mathcal{H}_{-1}, \hat{c}_{\mathbf{k}, \sigma}] \\ &= e^2 A^2 B^2 (k_y^2 + k_z^2 + 2k_y k_z \sin(\phi)) \Psi_{\mathbf{k}}^\dagger \tau_z \Psi_{\mathbf{k}} + \\ &\quad \frac{e^2 A^2 v^2}{4} \Psi_{\mathbf{k}}^\dagger \tau_z \Psi_{\mathbf{k}} + e^2 A^2 Bv (k_z + k_y \sin(\phi)) \Psi_{\mathbf{k}}^\dagger \tau_x \Psi_{\mathbf{k}}. \end{aligned} \quad (5)$$

Then the full form of the effective Hamiltonian is expressed as  $\mathcal{H}_{\text{eff}}(\mathbf{k}) = \sum_{\mathbf{k}} \hat{\Psi}_{\mathbf{k}}^\dagger \hat{H}_{\mathbf{k}} \hat{\Psi}_{\mathbf{k}}$  with

$$\begin{aligned} \hat{H}_{\mathbf{k}} &= [\tilde{m} - Bk^2 - i(\gamma_1 k_y \sin(\phi) + \gamma_1 k_z)] \tau_x + \lambda k_y \tau_y \\ &\quad + [vk_z + i(\gamma_2 - \gamma_3(k_y^2 + k_z^2 + 2k_y k_z \sin(\phi)))] \tau_z, \end{aligned} \quad (6)$$

where  $\gamma_1 = 4e^2 A^2 Bv\gamma/\omega^2$  and  $\gamma_2 = \gamma + e^2 A^2 v^2/\omega^2$  and  $\gamma_3 = 4e^2 A^2 B^2 \gamma/\omega^2$ . We can rewrite the Hamiltonian in a more compact form,

$$\hat{H}_{\mathbf{k}} = \mathbf{d}(\mathbf{k}) \cdot \boldsymbol{\sigma}, \quad \mathbf{d} \in \mathbb{C}^3, \quad (7)$$

where the vector  $\mathbf{d}$  can be decomposed into real and imaginary parts according to  $\mathbf{d} = \mathbf{d}_R + i\mathbf{d}_I$ . Then the eigenvalues and thus energies take a general form,

$$E_{\pm}^2 = \mathbf{d}_R^2 - \mathbf{d}_I^2 + 2i\mathbf{d}_R \cdot \mathbf{d}_I. \quad (8)$$

For the non-Hermitian system we consider,  $E_{\pm} = \sqrt{A(\mathbf{k})} e^{i\theta/2}$ , where  $A(\mathbf{k}) = \sqrt{(\mathbf{d}_R^2 - \mathbf{d}_I^2)^2 + 4(\mathbf{d}_R \cdot \mathbf{d}_I)^2}$  and  $\theta = \arctan[(\mathbf{d}_R^2 - \mathbf{d}_I^2)/2(\mathbf{d}_R \cdot \mathbf{d}_I)]$ . Thus the eigenvalues of Hamiltonian possess two branches then acquire a nontrivial energy vorticity.

We calculate the band structure from the Floquet Hamiltonian defined in Eq. (6). The results are shown in Fig. 1. The nodal points in the spectrum are described by solutions to the equations,

$$\mathbf{d}_R^2 - \mathbf{d}_I^2 = 0, \quad \mathbf{d}_R \cdot \mathbf{d}_I = 0. \quad (9)$$

In the high-frequency limit  $\omega \gg 1$ , the term dependent on  $\omega$  can be neglected and the energy spectrum is approximated by,

$$E = \pm \sqrt{(\tilde{m} - Bk^2)^2 + v^2 k_z^2 - \gamma^2 + 2ivk_z \gamma}. \quad (10)$$

When  $\gamma < m$ , two ERs characterized by  $Bk^2 = \tilde{m} \pm \gamma$  lie in the  $k_z = 0$  plane, as shown in Fig.1 (a). The inner ER shrinks as  $\gamma$  increases, and vanishes beyond a critical value of  $\gamma = \tilde{m}$  where it becomes an EP. As the driving frequency  $\omega$  decreases and the system goes into the low-frequency regime, the structure of the exceptional solutions dramatically changes. We consider  $\gamma = 0.5\tilde{m}$  as a typical example. The inner ER extends and cuts the outer ER to form an unconcentric dipolar pair, as illustrated in Fig. 1 (b). Fig.1 (c) shows the band-touching for  $\omega/A \sim 1$  where higher-order corrections lead to more remarkable modifications. The condition  $\mathbf{d}_R \cdot \mathbf{d}_I = 0$  gives two more solutions  $k_x = \pm \sqrt{\tilde{m}\gamma_1 - \gamma_2}$ , except for  $k_z = 0$ . With  $k_z = 0$ ,  $\mathbf{d}_R^2 - \mathbf{d}_I^2 = 0$  reduces to,

$$k_x^2 = \frac{\tilde{m}}{B} - k_y^2 \pm \frac{\sqrt{B^2(\gamma_2^2 - 2\gamma_2\gamma_3 k_y^2 + \gamma_3^2 k_y^4 - \lambda^2 k_y^2)}}{B^2}. \quad (11)$$

In particular, for the critical non-Hermiticity  $\gamma = \tilde{m}$  where an ER accompanied with a single EP appears in the spectrum in high-frequency limit, the inner EP could be tuned into an ER under the periodic driving.

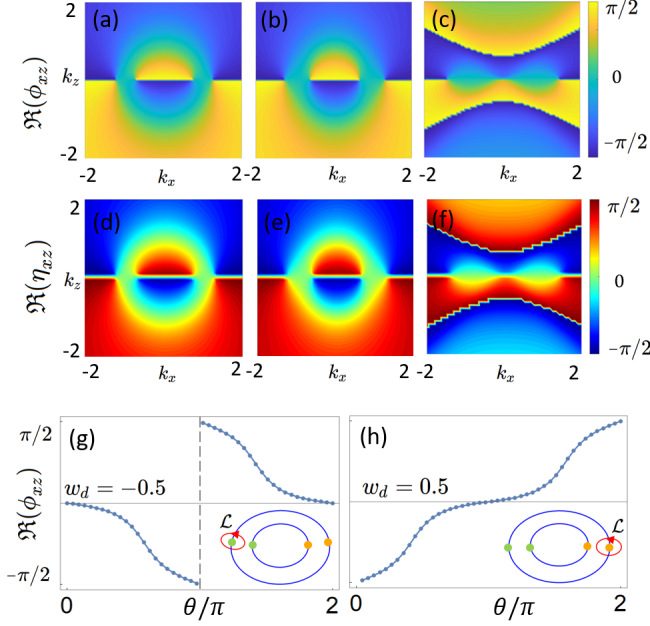


FIG. 2: (a), (b) and (c) respectively show the relative phase  $\phi_{xz}(k_x, k_z)$  with  $\tilde{m} = 1$ ,  $B = 1$ ,  $v = 1$ ,  $\gamma = 0.5$  and (a)  $\omega/A = 10$ , (b)  $\omega/A = 2$  and (c)  $\omega/A = 1$ ; (b), (c) and (d) respectively show the relative phase  $\eta_{xz}(k_x, k_z)$  of spin textures for an evolution time  $T = 20$ ; (g) and (h) show the winding number extracted from the loops encircling the two exceptional points on the inner ER.

*Topological characterization*—The exceptional ring and exceptional point are topological defects which can be characterized by a quantized Berry phase,

$$\gamma_B = \oint_{2\mathcal{L}} i \langle \tilde{u}(\mathbf{k}) | \partial_{\mathbf{k}} u(\mathbf{k}) \rangle d\mathbf{k}, \quad (12)$$

where  $\langle \tilde{u}(\mathbf{k}) |$  and  $|u(\mathbf{k})\rangle$  are left and right eigenvectors of the Hamiltonian Eq. (6) respectively; the path  $2\mathcal{L}$  travels across the ring twice. The path  $2\mathcal{L}$  forms a closed loop on the Riemann surface defined by  $E(\theta)$  [17], and the system returns to its original state after wrapping the ER twice.

Without loss of generality, we consider a path in the  $k_y = 0$  plane. For the two-band model we consider, the Berry phase can be associated to a winding number with the relation  $\gamma_B = 2\pi w$ , where

$$w = \frac{1}{2\pi} \oint_{\mathcal{L}} \partial_{\mathbf{k}} \phi_{xz}(\mathbf{k}) d\mathbf{k}, \quad (13)$$

with  $\phi_{xz}(\mathbf{k}) \equiv \arctan(h_x/h_z)$ . The winding number can be experimentally detected with a dynamic approach from the long-time average of spin textures [76, 77]. The spin textures are defined as the expectation values of the Pauli matrices  $\langle \sigma_j(\mathbf{k}, t) \rangle = \langle \tilde{u}_{\mathbf{k}} | \sigma_j | u_{\mathbf{k}} \rangle / \langle \tilde{u}_{\mathbf{k}} | u_{\mathbf{k}} \rangle$  in a biorthogonal formalism. The dynamic winding number is defined by the spin vector

$$w_d = \frac{1}{2\pi} \oint_{\mathcal{L}} \partial_{\mathbf{k}} \eta_{ij}(\mathbf{k}) d\mathbf{k}, \quad (14)$$

where  $\eta_{ij}(\mathbf{k}) \equiv \arctan(\bar{\sigma}_j/\bar{\sigma}_i)$  and  $\bar{\sigma}_j = \frac{1}{T} \int_0^T \langle \sigma_j(\mathbf{k}, t) \rangle dt$ . In the long-time limit, this dynamic winding number is equivalent to the winding number  $w = \lim_{T \rightarrow \infty} w_d$ . Only the real part of the phase  $\eta_{ij}(\mathbf{k})$  has nontrivial contributions and it can be decomposed to the sum of two observables [80],

$$\Re(\eta_{ij}(\mathbf{k})) = \frac{1}{2} (\phi_{ij}^{RR} + \phi_{ij}^{LL}) + n \frac{\pi}{2}, \quad (15)$$

where  $\phi_{ij}^{RR} = \arctan(\langle \tilde{u} | \sigma_i | u \rangle / \langle u | \sigma_j | u \rangle)$  and  $\phi_{ij}^{LL} = \arctan(\langle \tilde{u} | \sigma_i | \tilde{u} \rangle / \langle \tilde{u} | \sigma_j | \tilde{u} \rangle)$ .

As shown in Fig. 2, the ERs are characterized by the winding number along an  $S^1$  loop which interlinks with them. The fact that the winding number takes value out of  $\mathbb{Z}/2$  can be attributed to the net vorticity of this NH system. Furthermore, numerical simulations show that the dynamical winding number has good agreement with the winding number, as shown in Fig. 2 (d)-(f).

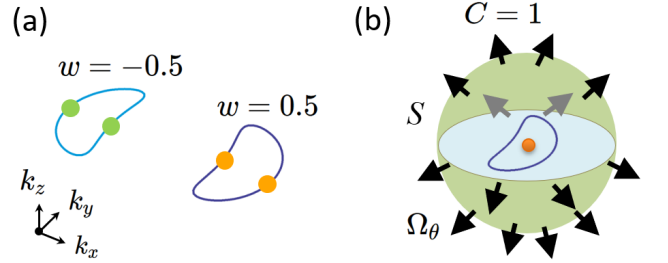


FIG. 3: (a) The winding number of the ER, which is 0.5 for integral loop which interlinks with the ER, and 1 for that encircling the ER, (b) The Chern number of the ER. The ER is analogous to the Weyl point in the Hermitian case, indicated as colored dot in (b).

When the system goes into the low-frequency regime, the double concentric ERs are deformed as a dipolar pair with two pole ERs which carry opposite topological charges  $w = \pm 1$  defined on the loop encircling the whole ER [indicated in Fig.3 (a)]. The net winding number implies that the ER is protected by a Chern number,

$$C = \frac{1}{2\pi} \oint_S \Omega_\theta(\mathbf{k}) \cdot d\mathbf{S} \quad (16)$$

where  $\Omega_\theta(\mathbf{k}) = i \langle \nabla_{\mathbf{k}} \tilde{u}_\theta(\mathbf{k}) | \times | \nabla_{\mathbf{k}} u_\theta(\mathbf{k}) \rangle$  is the Berry curvature and  $S$  encloses whole single ER, as illustrated in Fig.3 (b). Calculation shows that  $C = \pm 1$ .

*Hall conductivity*.—The light beam is incident along x direction, thus we are interested in the  $yz$ -component of the Hall response  $\sigma_{yz}$ . As suggested by previous works [74, 75], the Hall conductivity of a generic two-band non-Hermitian Hamiltonian with form of Eq. (7) is given by

$$\sigma_{yz} = -\frac{e^2}{h} \int \frac{d^3k}{(2\pi)^3} \text{Re}[\hat{\mathbf{d}} \cdot \left( \frac{\partial \hat{\mathbf{d}}}{\partial k_y} \times \frac{\partial \hat{\mathbf{d}}}{\partial k_z} \right) \cdot \frac{\pi}{2} \text{sgn}(\text{Re } \mathbf{d})], \quad (17)$$

where  $\hat{\mathbf{d}} = \mathbf{d}/|\mathbf{d}|$ . With components considered in Eq.(6), the Hall conductivity takes the following explicit form:

$$\begin{aligned} \sigma_{yz} = & -\frac{e^2}{h} \int \frac{d^3k}{(2\pi)^3} \text{Re}[-\gamma_1\gamma_2\lambda + mv\lambda - Bvk_x^2\lambda - \\ & \gamma_1\gamma_3k_y^2\lambda + Bvk_y^2\lambda + 2iB\gamma_2k_z\lambda - 2i\gamma_3mk_z\lambda + \\ & 2iB\gamma_3k_x^2k_z\lambda - \gamma_1\gamma_3k_z^2\lambda + Bvk_z^2\lambda]/E_+^3 \cdot \frac{\pi}{2} \text{sgn}(\text{Re } \mathbf{d}). \end{aligned} \quad (18)$$

We numerically calculate the integral, and the results are shown in Fig. 4. A transition of the Hall conductivity from 0 to finite values appears when the dipolar pair of the ERs forms, which distinguishes from the Hermitian case where  $\sigma_{yz}$  is always nonzero under the driven field. And  $\sigma_{yz}$  is proportional to the distance between the two ERs, which is reminiscent of the results in Ref. [49]. Furthermore, it is readily seen that the Hall conductivity decreases as the strength of non-Hermiticity increases.

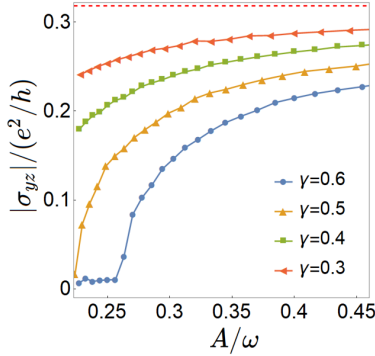


FIG. 4: The dependence of Hall conductivity on the frequency  $A/\omega$  of periodic driving. The parameters are  $\tilde{m} = 1$ ,  $B = 1$ ,  $v = 1$ ,  $\phi = 0$ . The Dashed line shows the value of  $\sigma_{yz}$  in Hermitian limit  $\sigma_0 = e^2/\pi h$ .

*Quantum simulation with a quantum spin system.*—To simulate the dynamics of the Hamiltonian  $\hat{H}_{\mathbf{k}}$ , an ancilla qubit is required to dilate  $\hat{H}_{\mathbf{k}}$  into a Hermitian Hamiltonian  $\hat{H}_d(t)$  [72]. The evolution of the dilated system  $\hat{H}_d(t)$  is governed by the Schrödinger equation,

$$i\frac{d}{dt}|\Psi(t)\rangle = \hat{H}_d(t)|\Psi(t)\rangle, \quad (19)$$

where  $|\Psi(t)\rangle$  is the state of the combined system. The essential idea that allows the exclusive dilation is to restrict the measurement results to those with a specific output for the ancilla qubit. In such a post-selection scenario, it's convenient to write the state  $|\Psi(t)\rangle$  in a form of

$$|\Psi(t)\rangle = |\psi(t)\rangle|-\rangle_a + \eta(t)|\psi(t)\rangle|+\rangle_a, \quad (20)$$

where  $|-\rangle_a$  and  $|+\rangle_a$  form an orthonormal basis of the ancilla qubit and here are chosen to be the eigenstates of  $\tau_y$  with  $|-\rangle = (|0\rangle - i|1\rangle)/\sqrt{2}$  and  $|+\rangle = -i(|0\rangle + i|1\rangle)/\sqrt{2}$ . And after the evolution, a  $-\pi/2$  pulse is applied and only the measurement results with no jump outside the sub-manifold  $|\psi\rangle|1\rangle_a$  are post-selected.

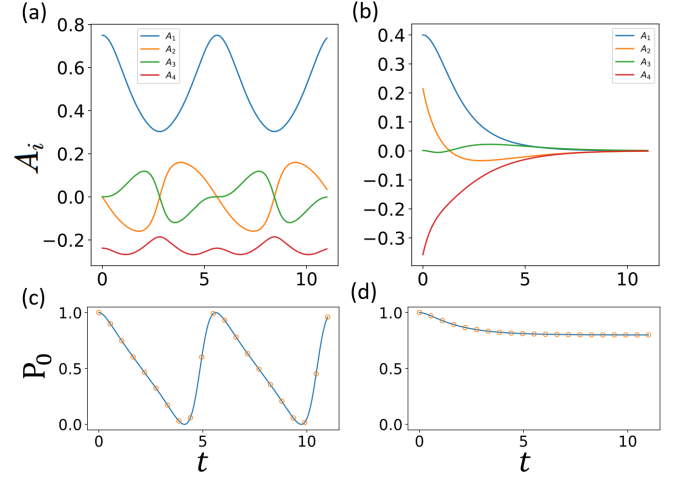


FIG. 5: (a) and (b) Parameters  $A_i(t)$  in the dilated Hamiltonian. In general  $B_i \neq 0$ , but for parameters considered here  $B_i = 0$ . (c) and (d) The population on state  $|0\rangle$  at time  $t$ . The solid lines indicate the analytic results solved for the Schrödinger equation  $i\hbar\partial_t\psi = \hat{H}_{\mathbf{k}}\psi$ ; the circles indicate the numerical results solved for dilated Hamiltonian  $\hat{H}_d$ . The parameters in  $\hat{H}_{\mathbf{k}}$  are chosen as  $\tilde{m} = v = B = 1$  and (a,c)  $k_x^2 + k_y^2 = 0.25$ ,  $k_z = 0$ , (b,d)  $k_x^2 + k_y^2 = 0.6$ ,  $k_z = 0$ .

Note that the Hamiltonian  $\hat{H}_d(t)$  is not uniquely determined. One proper choice is

$$\hat{H}_d(t) = \Lambda(t) \otimes \mathbb{I} + \Gamma(t) \otimes \sigma_z, \quad (21)$$

where  $\Lambda(t) = \{\hat{H}_{\mathbf{k}}(t) + [i\frac{d}{dt}\eta(t) + \eta(t)\hat{H}_{\mathbf{k}}(t)]\eta(t)\}M^{-1}(t)$  and  $\Gamma(t) = i[\hat{H}_{\mathbf{k}}(t)\eta(t) - \eta(t)\hat{H}_{\mathbf{k}}(t) - i\frac{d}{dt}\eta(t)]M^{-1}(t)$ . The time-dependent operator  $M(t)$  takes the form  $M(t) = \eta^\dagger\eta + I$ . And we can expand  $\Lambda(t)$  and  $\Gamma(t)$  in terms of the Pauli operators and rewrite  $\hat{H}_d(t)$  as

$$\begin{aligned} \hat{H}_d = & A_1(t)\sigma_x \otimes \mathbb{I} + A_2(t)\mathbb{I} \otimes \sigma_z + A_3(t)\sigma_y \otimes \sigma_z + A_4(t)\sigma_z \otimes \sigma_z \\ & + B_1(t)\mathbb{I} \otimes \mathbb{I} + B_2(t)\sigma_y \otimes \mathbb{I} + B_3(t)\sigma_z \otimes \mathbb{I} + B_4(t)\sigma_x \otimes \sigma_z. \end{aligned} \quad (22)$$

Figures 5 (a) and (b) show the time-dependent parameters  $A_i$  ( $i = 1-4$ ). Without loss of generality, here we only take the Hamiltonian in high-frequency limit as an example. The four level system described by the Hamiltonian  $\hat{H}_d$  could be encoded in the ground state manifold of electron spin and nuclear spin in a NV center, or alternatively, other quantum platforms such as trapped ion, Rydberg atom, and superconducting circuit. As shown in Fig. 5 (c) and (d), we demonstrate that the dynamics of the NH nodal-line semimetal can be revealed in the post-selected state population, which allows us to reconstruct the topological information from the spin textures. In experiments, microwave pulses and two radio-frequency pulses could be applied to couple the ground states of a NV center. For the coupling strength tuned to  $\sim 600$  kHz, the dynamical process in Fig. 5 (c,d) can happen within  $10 \mu\text{s}$ , which is feasible with current technology.

*Conclusions.*—In summary, we have proposed a scheme to realize tunable exceptional rings in terms of Floquet engineering. As the driven frequency changes, a dipolar pair of ERs protected by opposite Chern numbers can be created from the NH semimetal with double concentric ERs. This transition process is accompanied by the emergency of a non-zero Hall conductivity. Furthermore, we explore possible realization with synthetic quantum matter, which do not require controlling an open system. The proposed system would provide a promising platform for elaborating NH topology which might be elusive in nature.

*Note added.*—When we prepare our manuscript, we became aware of a related eprint by A. Banerjee and A. Narayan [82].

### Acknowledgments

The authors thank S. L. Zhu for useful discussions. The work was supported by the National Natural Science Foundation of China (Grants No. 91636218 and No. U1801661) and the National Key Research and Development Program of China (Grants No. 2016YFA0301803).

### Appendix A: Derivation details

In this section, we give the detailed derivation of the micromotion term of Eq. (3) in the main text. We recall the full form of the first-order component of the Floquet Hamiltonian,

$$\mathcal{H}_{+1} = -\Psi_{\mathbf{k}}^{\dagger} [eAB(k_y - ie^{i\phi})\tau_x + i\frac{evA}{2}e^{i\phi}\tau_z] \Psi_{\mathbf{k}}, \quad (\text{A1})$$

$$\mathcal{H}_{-1} = -\Psi_{\mathbf{k}}^{\dagger} [eAB(k_y + ie^{-i\phi})\tau_x - i\frac{evA}{2}e^{-i\phi}\tau_z] \Psi_{\mathbf{k}}, \quad (\text{A2})$$

expanded as

$$\begin{aligned} \mathcal{H}_{+1} = & -[eAB(k_y - ie^{i\phi})(\hat{c}_{\mathbf{k},a}^{\dagger}\hat{c}_{\mathbf{k},b} + \hat{c}_{\mathbf{k},b}^{\dagger}\hat{c}_{\mathbf{k},a}) + \\ & i\frac{evA}{2}e^{i\phi}(\hat{c}_{\mathbf{k},a}^{\dagger}\hat{c}_{\mathbf{k},a} - \hat{c}_{\mathbf{k},b}^{\dagger}\hat{c}_{\mathbf{k},b})], \end{aligned} \quad (\text{A3})$$

$$\begin{aligned} \mathcal{H}_{-1} = & -[eAB(k_y + ie^{-i\phi})(\hat{c}_{\mathbf{k},a}^{\dagger}\hat{c}_{\mathbf{k},b} + \hat{c}_{\mathbf{k},b}^{\dagger}\hat{c}_{\mathbf{k},a}) - \\ & i\frac{evA}{2}e^{-i\phi}(\hat{c}_{\mathbf{k},a}^{\dagger}\hat{c}_{\mathbf{k},a} - \hat{c}_{\mathbf{k},b}^{\dagger}\hat{c}_{\mathbf{k},b})]. \end{aligned} \quad (\text{A4})$$

And the commutators are given by

$$[\mathcal{H}_{+1}, \hat{c}_{\mathbf{k},a}] = eAB(k_y - ik_z e^{i\phi})\hat{c}_{\mathbf{k},b} + i\frac{evA}{2}e^{i\phi}\hat{c}_{\mathbf{k},a}, \quad (\text{A5})$$

$$[\mathcal{H}_{+1}, \hat{c}_{\mathbf{k},a}]^{\dagger} = eAB(k_y + ik_z e^{-i\phi})\hat{c}_{\mathbf{k},b}^{\dagger} - i\frac{evA}{2}e^{-i\phi}\hat{c}_{\mathbf{k},a}^{\dagger}. \quad (\text{A6})$$

$$[\mathcal{H}_{+1}, \hat{c}_{\mathbf{k},b}] = eAB(k_y - ik_z e^{i\phi})\hat{c}_{\mathbf{k},a} - i\frac{evA}{2}e^{i\phi}\hat{c}_{\mathbf{k},b}, \quad (\text{A7})$$

$$[\mathcal{H}_{+1}, \hat{c}_{\mathbf{k},b}]^{\dagger} = eAB(k_y + ie^{-i\phi})\hat{c}_{\mathbf{k},a}^{\dagger} + i\frac{evA}{2}e^{-i\phi}\hat{c}_{\mathbf{k},b}^{\dagger}. \quad (\text{A8})$$

By inserting Eq. (A5) and (A6) into Eq. (3), we have

$$\begin{aligned} \frac{2i\gamma}{\omega^2} [\mathcal{H}_{+1}, \hat{c}_{\mathbf{k},a}]^{\dagger} [\mathcal{H}_{+1}, \hat{c}_{\mathbf{k},a}] = & \\ \frac{2i\gamma}{\omega^2} [e^2 A^2 B^2 (k_y^2 + k_z^2 - 2k_y k_z \sin \phi) \hat{c}_{\mathbf{k},b}^{\dagger} \hat{c}_{\mathbf{k},b} + & \\ \frac{e^2 A^2 B v}{2} (ik_y e^{i\phi} - k_z) \hat{c}_{\mathbf{k},b}^{\dagger} \hat{c}_{\mathbf{k},a} + \frac{e^2 A^2 v^2}{4} \hat{c}_{\mathbf{k},a}^{\dagger} \hat{c}_{\mathbf{k},a} - & \\ \frac{e^2 A^2 B v}{2} (ik_y e^{-i\phi} + k_z) \hat{c}_{\mathbf{k},a}^{\dagger} \hat{c}_{\mathbf{k},b}. & \end{aligned} \quad (\text{A9})$$

By inserting Eq. (A7) and (A8) into Eq. (3), we have

$$\begin{aligned} -\frac{2i\gamma}{\omega^2} [\mathcal{H}_{+1}, \hat{c}_{\mathbf{k},b}]^{\dagger} [\mathcal{H}_{+1}, \hat{c}_{\mathbf{k},b}] = & \\ -\frac{2i\gamma}{\omega^2} [e^2 A^2 B^2 (k_y^2 + k_z^2 - 2k_y k_z \sin \phi) \hat{c}_{\mathbf{k},a}^{\dagger} \hat{c}_{\mathbf{k},a} - & \\ \frac{e^2 A^2 B v}{2} (ik_y e^{i\phi} - k_z) \hat{c}_{\mathbf{k},a}^{\dagger} \hat{c}_{\mathbf{k},b} + \frac{e^2 A^2 v^2}{4} \hat{c}_{\mathbf{k},b}^{\dagger} \hat{c}_{\mathbf{k},b} + & \\ \frac{e^2 A^2 B v}{2} (ik_y e^{-i\phi} + k_z) \hat{c}_{\mathbf{k},b}^{\dagger} \hat{c}_{\mathbf{k},a}. & \end{aligned} \quad (\text{A10})$$

Collecting all terms in Eq. (A9) and Eq. (A10) gives

$$\begin{aligned} \sum_{\sigma} s \frac{2i\gamma}{\omega^2} [\mathcal{H}_{+1}, \hat{c}_{\mathbf{k},\sigma}]^{\dagger} [\mathcal{H}_{+1}, \hat{c}_{\mathbf{k},\sigma}] = & \\ -\frac{2i\gamma}{\omega^2} [e^2 A^2 B^2 (k_y^2 + k_z^2 - 2k_y k_z \sin \phi) - \frac{e^2 A^2 v^2}{4}] \Psi_{\mathbf{k}}^{\dagger} \tau_z \Psi_{\mathbf{k}} & \\ -\frac{2i\gamma}{\omega^2} \frac{e^2 A^2 B v}{2} [2k_y \sin \phi + k_z] \Psi_{\mathbf{k}}^{\dagger} \tau_x \Psi_{\mathbf{k}}. & \end{aligned} \quad (\text{A11})$$

In the same way we can obtain that,

$$[\mathcal{H}_{-1}, \hat{c}_{\mathbf{k},\sigma}]^{\dagger} [\mathcal{H}_{-1}, \hat{c}_{\mathbf{k},\sigma}] = [\mathcal{H}_{+1}, \hat{c}_{\mathbf{k},\sigma}]^{\dagger} [\mathcal{H}_{+1}, \hat{c}_{\mathbf{k},\sigma}]. \quad (\text{A12})$$

- 
- [1] C. M. Bender and S. Boettcher, Real spectra in non-Hermitian Hamiltonians having P T symmetry, *Phys. Rev. Lett.* **80**, 5243 (1998).
- [2] E. J. Bergholtz, J. C. Budich, and F. K. Kunst, Exceptional Topology of Non-Hermitian Systems, arXiv:1912.10048 (2019).
- [3] A. Ghatak and T. Das, New topological invariants in non-Hermitian systems, *J. Phys. D: Appl. Phys.* **31**, 263001 (2019).
- [4] V. Kozii and L. Fu, Non-Hermitian topological theory of finite-lifetime quasiparticles: prediction of bulk Fermi arc due to exceptional point, arXiv:1708.05841 (2017).
- [5] T. Yoshida, R. Peters, and N. Kawakami, Exceptional rings in two-dimensional correlated systems with chiral symmetry, *Phys. Rev. B* **98**, 035141 (2018).
- [6] K. Kimura, T. Yoshida, and N. Kawakami, Chiral-symmetry protected exceptional torus in correlated nodal-line semi-metals, *Phys. Rev. B* **100**, 115124 (2019).
- [7] Y. Michishita and R. Peters, Equivalence of the effective non-hermitian Hamiltonians in the context of open quantum systems and strongly-correlated electron systems, arXiv:2001.09045 (2020).
- [8] A. A. Zyuzin and A. Y. Zyuzin, Flat band in disorder driven non-Hermitian Weyl semimetals, *Phys. Rev. B* **97**, 041203(R) (2018).
- [9] M. Papaj, H. Isobe, and L. Fu, Nodal arc of disordered Dirac fermions and non-Hermitian band theory, *Phys. Rev. B* **99**, 201107 (2019).
- [10] D. W. Zhang et al., Non-Hermitian topological Anderson insulators, *Sci. China-Phys. Mech. Astron.* **63**, 267062 (2020).
- [11] J. Li, et al., Observation of parity-time symmetry breaking transitions in a dissipative Floquet system of ultracold atoms, *Nat. Commun.* **10**, 855 (2019).
- [12] H. Jiang, et al., Interplay of non-Hermitian skin effects and Anderson localization in nonreciprocal quasiperiodic lattices, *Phys. Rev. B* **100**, 054301 (2019).
- [13] S. Klaiman, U. Günther, and N. Moiseyev, Visualization of branch points in p t-symmetric waveguides, *Phys. Rev. Lett.* **101**, 080402 (2008).
- [14] H. Zhou et al., Observation of bulk Fermi arc and polarization half charge from paired exceptional points, *Science*, **359**, 1009-1012 (2018).
- [15] A. Cerjan et al., Experimental realization of a Weyl exceptional ring, *Nat. Photonics*, **13**, 623-628 (2019).
- [16] K. Yokomizo and S. Murakami, Topological semimetal phase with exceptional points in 1D non-Hermitian systems, arXiv:2001.07348 (2020).
- [17] Y. Xu, S. T. Wang, and L. M. Duan, Weyl exceptional rings in a three-dimensional dissipative cold atomic gas, *Phys. Rev. Lett.* **118**, 045701 (2017).
- [18] H. Wang, J. Ruan, and H. Zhang, Non-Hermitian nodal-line semimetals with an anomalous bulk-boundary correspondence, *Phys. Rev. B* **99**, 075130 (2019).
- [19] J. C. Budich, et al., Symmetry-protected nodal phases in non-Hermitian systems, *Phys. Rev. B*, **99**, 041406 (2019).
- [20] J. Carlström and E.J. Bergholtz, Exceptional links and twisted Fermi ribbons in non-Hermitian systems, *Phys. Rev. A* **98**, 042114 (2018).
- [21] Z. Yang and J. Hu, Non-Hermitian Hopf-link exceptional line semimetals, *Phys. Rev. B* **99**, 081102 (2019).
- [22] J. Carlström, M. Stålhammar, J.C. Budich, and E.J. Bergholtz, Knotted Non-Hermitian Metals, *Phys. Rev. B* **99**, 161115(R) (2019).
- [23] X. Zhang, et al., Experimental observation of an exceptional surface in synthetic dimensions with magnon polaritons, *Phys. Rev. Lett.* **123**, 237202 (2019).
- [24] K. Yamamoto, M. Nakagawa, K. Adachi, et al., Theory of Non-Hermitian Fermionic Superfluidity with a Complex-Valued Interaction, *Phys. Rev. Lett.* **123**, 123601 (2019).
- [25] R. Okugawa and T. Yokoyama, Topological exceptional surfaces in non-Hermitian systems with parity-time and parity-particle-hole symmetries, *Phys. Rev. B* **99**, 041202 (2019).
- [26] D. Leykam, et al., Edge modes, degeneracies, and topological numbers in non-Hermitian systems, *Phys. Rev. Lett.* **118**, 040401 (2017).
- [27] H. Shen, B. Zhen, and L. Fu, Topological band theory for non-Hermitian Hamiltonians, *Phys. Rev. Lett.* **120**, 146402 (2018).
- [28] Z. Gong, et al., Topological phases of non-Hermitian systems, *Phys. Rev. X* **8** 031079 (2019).
- [29] K. Kawabata, et al., Symmetry and topology in non-Hermitian physics, *Phys. Rev. X* **9**, 041015 (2019).
- [30] Q. Zhang and B. Wu, Monopoles in non-Hermitian systems, *Phys. A: Math. Theor.* **53**, 065203 (2019).
- [31] Z. Yang, et al., Fermion doubling theorems in 2D non-Hermitian systems, arXiv:1912.02788 (2019).
- [32] S. Yao and Z. Wang, Edge states and topological invariants of non-Hermitian systems, *Phys. Rev. Lett.* **121**, 086803 (2018).
- [33] F. Song, S. Yao, and Z. Wang, Non-Hermitian skin effect and chiral damping in open quantum systems, *Phys. Rev. Lett.* **123**, 170401 (2019).
- [34] L. Li, C. H. Lee, and J. Gong, Topology-Induced Spontaneous Non-reciprocal Pumping in Cold-Atom Systems with Loss, arXiv:1910.03229 (2019).
- [35] C. H. Lee and R. Thomale, Anatomy of skin modes and topology in non-Hermitian systems, *Phys. Rev. B* **99**, 201103 (2019).
- [36] C. H. Lee, L. Li, and J. Gong, Hybrid higher-order skin-topological modes in nonreciprocal systems, *Phys. Rev. Lett.* **123** 016805 (2019).
- [37] N. Okuma, et al., Topological Origin of Non-Hermitian Skin Effects, arXiv:1910.02878 (2019).
- [38] S. Yao, F. Song, and Z. Wang, Non-hermitian chern bands, *Phys. Rev. Lett.* **121** 136802 (2018).
- [39] F. K. Kunst, et al., Biorthogonal bulk-boundary correspondence in non-Hermitian systems, *Phys. Rev. Lett.* **121**, 026808 (2018).
- [40] K. Yokomizo and S. Murakami, Non-bloch band theory of non-Hermitian systems, *Phys. Rev. Lett.* **123**, 066404 (2019).
- [41] K. Zhang, Z. Yang, and C. Fang, Correspondence between winding numbers and skin modes in non-hermitian systems, arXiv:1910.01131 (2019).
- [42] A. A. Burkov, M. D. Hook, and L. Balents, Topological nodal semimetals, *Phys. Rev. B* **84**, 235126 (2011).
- [43] O. Trker and S. Moroz, Weyl nodal surfaces, *Phys. Rev. B* **97** 075120 (2018).
- [44] D. W. Zhang et al., Topological quantum matter with cold atoms, *Adv. Phys.* **67**, 253 (2018).

- [45] V.M. Pereira, et al., Tight-binding approach to uniaxial strain in graphene, *Phys. Rev. B* **80**, 045401 (2009)
- [46] S. L. Zhu, B. Wang, and L.-M. Duan, Simulation and Detection of Dirac Fermions with Cold Atoms in an Optical Lattice, *Phys. Rev. Lett.* **98**, 260402 (2007).
- [47] L. Tarruell et al., Creating, moving and merging Dirac points with a Fermi gas in a tunable honeycomb lattice, *Nature* **483**, 302 (2012).
- [48] D. W. Zhang, et al., Relativistic quantum effects of Dirac particles simulated by ultracold atoms, *Frontiers of Physics*, **7**, 31 (2012).
- [49] Z. Yan and Z. Wang, Tunable Weyl points in periodically driven nodal line semimetals, *Phys. Rev. Lett.* **117**, 087402 (2016).
- [50] A. Narayan, Tunable point nodes from line-node semimetals via application of light, *Phys. Rev. B* **94**, 041409 (2016).
- [51] L. Li, C. H. Lee, and J. Gong, Realistic Floquet semimetal with exotic topological linkages between arbitrarily many nodal loops, *Phys. Rev. Lett.* **121**, 036401 (2018).
- [52] G. Salerno, N. Goldman, and G. Palumbo, Floquet-engineering of nodal rings and nodal spheres and their characterization using the quantum metric, arXiv:1912.00930, (2019).
- [53] A. Eckardt, Colloquium: Atomic quantum gases in periodically driven optical lattices, *Rev. Mod. Phys.* **89**, 011004 (2017).
- [54] S. Yao, Z. Yan, Z. Wang, et al. Topological invariants of Floquet systems: General formulation, special properties, and Floquet topological defects, *Phys. Rev. B* **96**, 195303 (2017).
- [55] L. Zhou, J. Gong, Non-Hermitian Floquet topological phases with arbitrarily many real-quasienergy edge states, *Phys. Rev. B* **98**, 205417 (2018).
- [56] L. Zhou, Non-Hermitian Floquet topological superconductors with multiple Majorana edge modes, *Phys. Rev. B* **101**, 014306 (2020).
- [57] Wu H, An J., Floquet Topological Phases of Non-Hermitian Disordered Systems, arXiv:2003.08055 (2020). *Phys. Rev. A* **95**, 063616 (2017).
- [58] D. W. Zhang et al., Generalized Hofstadter model on a cubic optical lattice: From nodal bands to the three-dimensional quantum Hall effect, *Phys. Rev. A* **95**, 043619 (2017).
- [59] Z. Li et al., Dynamics of Weyl quasiparticles in an optical lattice, *Phys. Rev. A* **94**, 043617 (2016)
- [60] D. W. Zhang et al., Quantum simulation of exotic PT-invariant topological nodal loop bands with ultracold atoms in an optical lattice, *Phys. Rev. A* **93**, 043617 (2016).
- [61] F. Mei et al., Topological insulator and particle pumping in a one-dimensional shaken optical lattice, *Phys. Rev. A* **90**, 063638 (2014).
- [62] G. Liu et al., Topological superfluid transition induced by a periodically driven optical lattice, *Phys. Rev. A* **86**, 013639 (2012).
- [63] X. Zhu, H. Ramezani, C. Shi, J. Zhu, and X. Zhang, PT-symmetric acoustics. *Phys. Rev. X* **4**, 031042 (2014).
- [64] B.I. Popa and S. A. Cummer, Non-reciprocal and highly nonlinear active acoustic metamaterials. *Nat. Commun.* **5**, 3398 (2014).
- [65] L. Xiao, et al., Observation of non-hermitian bulk-boundary correspondence in quantum dynamics, arXiv:1907.12566 (2019).
- [66] K. Wang, et al., Observation of emergent momentumtime skyrmions in paritytime-symmetric non-unitary quench dynamics, *Nat. Commun.*, **10**, 2293 (2019).
- [67] S. Diehl, et al., Topology by dissipation in atomic quantum wires, *Nature Phys.* **7**, 971-977 (2011).
- [68] Y. Takasu, T. Yagami, Y. Ashida, PT-symmetric non-Hermitian quantum many-body system using ultracold atoms in an optical lattice with controlled dissipation, arXiv: 2004.05734 (2020).
- [69] U. Günther and B. F. Samsonov, Naimark-dilated PT-symmetric brachistochrone. *Phys. Rev. Lett.* **101**, 230404 (2008).
- [70] M. Huang, et al., Simulating broken PT-symmetric Hamiltonian systems by weak measurement, *Phys. Rev. Lett.* **123**, 080404 (2019).
- [71] D. J. Zhang, Q. Wang, and J. Gong, Time-dependent PT-symmetric quantum mechanics in generic non-Hermitian systems, *Phys. Rev. A* **100**, 062121 (2019).
- [72] Y. Wu, et al., Observation of parity-time symmetry breaking in a single-spin system, *Science*, **364**, 878-880 (2019).
- [73] W. Liu, Y. Wu, C. Duan, et al., Dynamically encircling an exceptional point in a real quantum system, arXiv: 2002.06798 (2020).
- [74] M. R. Hirsbrunner, T. M. Philip, and M. J. Gilbert, Topology and observables of the non-Hermitian Chern insulator, *Phys. Rev. B*, **100**, 081104 (2019).
- [75] Y. Chen and H. Zhai, Hall conductance of a non-Hermitian Chern insulator, *Phys. Rev. B* **98**, 245130 (2018)
- [76] B. Zhu, et al., Dynamic winding number for exploring band topology, arXiv:1907.11348 (2019).
- [77] L. Zhou, Dynamical characterization of non-Hermitian Floquet topological phases in one dimension, *Phys. Rev. B* **100** 184314 (2019).
- [78] The presence of the Langevin force ensures the unitary of quantum operators, for details see Ref. [73].
- [79] L. Pan, X. Chen, Y. Chen, and H. Zhai, Non-Hermitian Linear Response Theory, arXiv:1909.12516 (2019).
- [80] C. Yin, H. Jiang, L. Li, R. L., and S. Chen, Geometrical meaning of winding number and its characterization of topological phases in one-dimensional chiral non-Hermitian systems, *Phys. Rev. A* **97**, 052115 (2018)
- [81] Y. Chen, L. Pan, H. Zhai, unpublished.
- [82] A. Banerjee and A. Narayan, Controlling Exceptional Points with Light, arXiv:2004.12606 (2020).